Enzalutamide-induced PTH1R-mediated TGFBR2 decrease in osteoblasts contributes to resistance in bone-metastatic prostate cancer

Shang Su[1#], Jingchen Cao[1#], Xiangqi Meng[1, 2#], Ruihua Liu[1, 3], Alexandra Vander Ark[1], Erica Woodford[1], Reian Zhang[1, 4], Isabelle Stiver[1, 4], Xiaotun Zhang[5], Zachary B. Madaj[6], Megan J. Bowman[1,7], Haiquan Yu[3], Eric Xu[1], Xiaohong Li[1]*

[1]Center for Cancer and Cell Biology, [6]Bioinformatics & Biostatistics Core, Van Andel Institute, Grand Rapids, MI, 49503; [2] Current address: The Sixth Affiliated Hospital of Sun Yat-sen University, Guangzhou, 510655, China; [3]Inner Mongolia University, Hohhot, 010021, China; [4]University of Michigan, Ann Arbor, MI, 48109; [5]Anatomic/Clinical Pathology, Mayo Clinic, Rochester, MN, 55905; [7]Current address: Ball Horticultural Company, West Chicago, IL, 60185, USA;

Running title: Enzalutamide resistance due to TGFBR2 decrease in osteoblasts

Keywords: enzalutamide resistance, bone-metastatic prostate cancer, osteoblasts, TGFBR2, PTHrP/PTH1R

Financial support: This work was supported by R01CA230744.

 # These authors contributed equally.

***Corresponding author**: **Xiaohong Li**, Van Andel Institute, 333 Bostwick Ave. NE, Grand Rapids, MI 49503. Phone: +1-616-234-5267; E-mail: xiaohong.li@vai.org

Conflict of Interest Disclosure: The authors have declared that no conflicts of interest exist.

Abstract

Over 80% of prostate cancer patients in the United States die with bone metastases. Second-line hormonal therapies, such as enzalutamide, improve overall survival in about 50% of patients with bone metastasis, but almost all responsive patients eventually develop resistance to the drug. The mechanistic studies of resistance have largely focused on prostate cancer cells. In this study, we focused on the bone microenvironment niche for metastatic cancer cells. We found that enzalutamide significantly decreased the amount of the TGFBR2 receptor in osteoblasts, both *in vitro* and in patient samples. A knockout of *Tgfbr2* specifically in osteoblasts significantly induced bone metastasis. We showed that the enzalutamide-induced TGFBR2 decrease in osteoblast was mediated by up-regulated PTH1R, which resulted in the TGFBR2 degradation, and blocking PTH1R rescued the TGFBR2 decrease. We also found that PTH1R up-regulation by enzalutamide was correlated with increased *Pth1r* promoter occupancy by transcription factor NR2F1. Our findings highlight a potential enzalutamide-resistance mechanism through TGFBR2 decrease in osteoblasts, thus suggesting future PTH1R-blocking approaches to overcome enzalutamide resistance in PCa bone metastasis.

Introduction

Prostate epithelial cells depend on androgen for growth, and because androgen signaling stimulates most prostate cancer (PCa) cell growth, androgen deprivation therapy (ADT) is the first-line treatment for prostate cancer (1, 2). Enzalutamide, a second-generation small-molecule inhibitor of the androgen receptor (AR), has been approved for patients who develop castration-resistant PCa bone metastases (mCRPC) after ADT failure (3). In the United States, over 80% of PCa patients die with bone metastases (4).

Cancer cell resistance to enzalutamide has been found both in patients and in laboratory models (3). While most research has focused on the cancer cells themselves, little attention has been paid to the bone microenvironment in which metastatic PCa cells prosper. By identifying the intrinsic changes or downstream molecular events in the bone microenvironment that result from enzalutamide treatment, specifically in the niche-forming cells such as osteoblasts, we may develop a novel therapeutic strategy to overcome enzalutamide resistance in PCa bone metastasis and thus improve therapeutic outcomes.

Previously, we showed that osteoblast-specific knockout of the TGF-β type II receptor gene (*Tgfbr2*) stimulated bone metastasis of AR-negative PCa cells (5). In this study, we proved that specific knockout of *Tgfbr2* in osteoblasts also promoted the bone metastasis of C4-2B cells, which are AR-positive cells that represent the majority of PCa cells in bone metastases (6). We observed that enzalutamide significantly reduced the expression of the TGF-β type II receptor (TGFBR2) in cultured osteoblasts, as well as in osteoblasts from PCa patients who had been treated with enzalutamide. We demonstrated that the events responsible for the enzalutamide-

induced TGFBR2 decrease in osteoblasts include the increased expression of the transcription factor NR2F1 (Nuclear Receptor Subfamily 2 Group F Member 1) followed by the NR2F1-activated increase in PTH1R (parathyroid hormone/parathyroid hormone-related peptide receptor), which induced TGFBR2 degradation. We also observed that the blocking of PTH1R rescued the TGFBR2 decrease. These data suggest an AR-PTH1R-TGFBR2 relationship for enzalutamide resistance and a possible strategy of using PTH1R blockade to overcome enzalutamide resistance in PCa bone metastasis.

Results and Discussion

The majority (80%) of PCa bone metastasis samples indeed express AR (6). Therefore, to determine whether the effect of enzalutamide on PCa depends on the microenvironment, we used AR-positive prostate cancer C4-2B cells, which are primarily isolated from bone metastasis and can be targeted by enzalutamide (7). One million C4-2B cells were injected subcutaneously into the flank (**Figure 1A**), intratibially (**Figure 1B)**, or orthotopically into the prostate **(Supplementary Figure 1**) of 5- to 6-wk-old male SCID mice. Enzalutamide (20 mg/kg body weight, through oral gavage) or vehicle was administered daily for consecutive 3 weeks. The C4-2B cells responded differently to enzalutamide in the different microenvironments. As expected, enzalutamide treatment significantly inhibited both subcutaneous and orthotopic C4-2B tumor growth (**Figure 1A** and **Supplementary Figure 1**). However, enzalutamide treatment had no effects on C4-2B bone lesion development in the mice intratibially injected (**Figure 1B)**. In other words, PCa cells in the bone microenvironment were resistant to enzalutamide, suggesting that the bone microenvironment likely caused their enzalutamide resistance.

We then focused our mechanistic studies on osteoblasts because metastatic PCa cells attach to them when colonizing in the bone (8, 9). It has been reported that cells grown in normal culture medium with 10% fetal bovine serum (FBS), which contains hormones such as androgen, mimics the very low level of androgen seen in the clinical situation under ADT (10). Therefore, we cultured murine MC3T3-E1 osteoblasts under these conditions to determine the effect of enzalutamide on osteoblasts. As mentioned above, we recently identified the role of osteoblast-specific *Tgfbr2* loss in promoting the bone metastasis of AR-negative PC-3 and DU145 cells (5). We then checked the expression of TGFBR2 in enzalutamide-treated osteoblasts and found a

significantly decreased amount of TGFBR2 at 24 to 72 h post enzalutamide treatment and at 20-μM and 40-μM doses. Enzalutamide at 40 μM also decreased TGFBR2 at 8 h and 12 h post enzalutamide treatment. No change in TGFBR2 was observed at 6 h of treatment (**Figure 2A**). To validate the specificity of enzalutamide effects, we knocked down the *Ar* gene in MC3T3-E1 osteoblast cells and observed a consistent decrease of TGFBR2 (**Figure 2B**), confirming the on-target effect of enzalutamide. The decrease of TGFBR2 by enzalutamide was also observed in the human fetal osteoblast cell line hFOB1.19 (**Figure 2C**), thus ruling out a species-specific bias. MC3T3-E1 osteoblasts were used for the subsequent experiments in this study.

To determine whether the *Tgfbr2* KO in osteoblasts had a promoting effect on bone metastasis of AR-positive PCa, we injected C4-2B cells into the tibiae of the previously established mouse model $Tgfbr2^{Col1CreERT}$ KO, in which *Tgfbr2* can be specifically knocked out in osteoblasts upon induction (5). C4-2B-induced mixed (osteoblastic and osteolytic) lesions (**Supplementary Figure 2A**), which is also a prominent pattern observed in most PCa patients (11). We found 21 out of 24 mice developed C4-2B cell-induced bone lesions in the tibiae in the $Tgfbr2^{Col1CreERT}$ KO group; in the $Tgfbr2^{FloxE2}$ (control) group, only 7 out 18 mice developed bone lesions (**Supplementary Figure 2B**). Statistical analysis suggested these two groups significantly ($p < 0.001$) differed in their proportions of the incidence of bone lesions, confirming that the TGFBR2 loss in osteoblasts promotes PCa bone metastasis.

To gain clinical insights into the osteoblast expressed TGFBR2 in PCa bone metastasis, we performed an IHC screen on TGFBR2 levels in a set of mCRPC patient tissue microarrays (UWTMA79) supported by the Prostate Cancer Biorepository Network (PCBN). Statistical

analysis showed the professionally rated expression scores of TGFBR2 in osteoblasts were significantly lower (p = 0.03) in patients who had received second-line hormonal therapy (n=13, either enzalutamide or an androgen biosynthesis inhibitor abiraterone in these cohorts) after androgen deprivation therapy than those who did not receive enzalutamide or abiraterone (n=32) (**Figure 2D, E**) (12). No difference of TGFBR2 expression in other cell types (such as tumor cells, stromal/fibroblasts, or osteoclasts) was observed in these patients (**Supplementary Table 1**). No correlations of TGFBR2 expression in osteoblasts were found for any other treatment group (such as bisphosphonate medicine Zometa, or antifungal ketoconazole) (**Supplementary Table 1**). The data suggested a potential drug resistance in PCa bone metastasis from the enzalutamide-induced TGFBR2 decrease in osteoblasts.

The decrease of TGFBR2 by enzalutamide in MC3T3-E1 cells was not observed until 8 h of treatment (see **Figure 2A**), suggesting an indirect effect. One previous study has shown that parathyroid hormone (PTH) activates PTH1R to recruit TGFBR2, which phosphorylates PTH1R and which together undergo endocytosis for protein degradation (13). Bone metastatic PCa cells are known to secrete factors such as PTHrP (parathyroid hormone-related protein), which could also bind and activate PTH1R but would give a distinct conformation relative to PTH-activated PTH1R (14, 15). This suggests that PTHrP could induce TGFBR2 degradation by activation of PTH1R.

To observe the dynamics of endogenous TGFBR2, we treated MC3T3-E1 cells with the protein synthesis inhibitor cycloheximide together with PTHrP. We found that both TGFBR2 and PTH1R were decreased to an undetectable level after 12 h of PTHrP treatment (**Figure 3A**).

TGF-β stimulation results in the phosphorylation of Smad2 (p-Smad2), the activation of downstream signaling, and the degradation of TGFBR2 through ubiquitination, so TGF-β treatment was used as a positive control for p-Smad2 up-regulation and TGFBR2 down-regulation (16). These data suggested that PTHrP, through activation of PTH1R, induced the down-regulation of TGFBR2 and its downstream signaling.

We then conducted a time-course treatment of enzalutamide on MC3T3-E1 cells and found that prior to the decrease of TGFBR2, enzalutamide treatment increased PTH1R (**Figure 3B**). PTH1R proteins were increased upon enzalutamide treatment at multiple time points from 2 to 24 h but were not affected at 48 h. The most significant increase in PTH1R was observed at 6 h, when there was no change of TGFBR2. TGFBR2 down-regulation was consistently observed at and after 24 h of treatment. These data suggested that enzalutamide might directly increase PTH1R, which subsequently result in the decrease of TGFBR2. We further observed a significant increase in *Pth1r* mRNA at early time points (before 6 h) upon enzalutamide treatment (**Figure 3C**), suggesting that PTH1R up-regulation is one of the early effects of enzalutamide on osteoblasts. When we treated C4-2B prostate cancer cells stably expressing TGFBR2 (termed as C4-2B/TGFBR2) or RAW264.7 osteoclasts with enzalutamide, however, PTH1R did not increase, although TGFBR2 did decrease at certain time points, suggesting that the mechanism by which enzalutamide-induced PTH1R-mediated TGFBR2 decrease only exist in osteoblasts (**Supplementary Figure 3**). Moreover, TGFBR2 expression in enzalutamide-treated osteoblasts was rescued by treatment with a small-molecule inhibitor of PTH1R, a neutralizing antibody against PTH1R, or a peptide antagonist of PTHrP (**Figure 3D**). These data

collectively demonstrated that PTH1R is a key player in the enzalutamide-induced TGFBR2 decrease.

Next, we aimed to determine the mechanism by which enzalutamide increased PTH1R in osteoblasts. As PTH1R was up-regulated at both the transcriptional and protein levels (see **Figure 3B, C**), the most likely explanation would be the enhanced transcriptional activation of *Pth1r* by transcription factor(s). We adopted a text-mining approach using MetaCore to search for candidates that are linked with both AR and PTH1R, and the top hit we got was Nuclear Receptor Subfamily 2 Group F Member 1 (NR2F1) (**Figure 4A**). NR2F1 was negatively associated with AR signaling and could activate the expression of *Pth1r* (17, 18). Indeed, we observed significant increases of both *Nr2f1* mRNA and NR2F1 protein in osteoblasts treated with enzalutamide (**Figure 4B, C**). We did not observe an increase of NR2F1 in RAW264.7 or C4-2B/TGFBR2 cells (**Supplementary Figure 3**). We downloaded the binding element information of NR2F1 (5-A/G-A/G-GGTCA-3) from the JASPAR database and searched the element across the upstream regulatory sequences of mouse *Pth1r* (**Figure 4D**) (19). There are at least three major transcript variants of mouse *Pth1r* (labeled as V1, V2, and V3, driven by at least three different promoters, as shown in **Figure 4D**); Promoter of V1 is considered absent or very weak in the bone while those of V2 and V3 are active in the bone (20). We found multiple NR2F1 binding elements at the promoters of each transcript variant. We designed several sets of primer (amplicons termed as c1, c2, and c3, as shown in **Figure 4D**) and conducted ChIP-qPCR to determine the occupancy of NR2F1 in the *Pth1r* promoter region. We found that NR2F1 bound to at least one of these promoter regions, and the occupancy was enhanced by enzalutamide, indicated by the elevated fold enrichment (**Figure 4D**). These data suggested that

enzalutamide induced PTH1R expression by enhancing the *Pth1r* promoter occupancy of NR2F1.

Our study highlights the importance of understanding the role of the tumor microenvironment in PCa bone metastasis and drug resistance by demonstrating a signaling regulatory axis of enzalutamide in osteoblasts. Distinct from the enzalutamide-induced AR signaling blockade and tumor growth suppression in the prostate and subcutaneous region, enzalutamide blockade of AR increased the *Pth1r* promoter occupancy of NR2F1, stimulating the expression of PTH1R, which in turn led to the degradation of TGFBR2 in the bone microenvironment (**Figure 4E**). Our data thus suggests promising approaches to overcome enzalutamide resistance by blocking PTH1R.

Methods

Animals, cells, proteins, and drugs

The genetically engineered mouse models, *Tgfbr2*^{FloxE2} and *Tgfbr2*^{Col1CreERT} knockout (KO), have been characterized and described previously(5). Briefly, the mice were generated by crossing collagen 1α2 promoter-driven CreERT (*Col1CreERT*) mice and *Tgfbr2*^{FloxE2} mice. To activate the Cre recombinase, the *Cre*$^{-}$ and *Cre*$^{+}$ littermates were injected with tamoxifen (10 mg/kg body weight) for five consecutive days. Between the 5th and 7th day after the last tamoxifen injection, the resulting *Tgfbr2*^{FloxE2} (control) and *Tgfbr2*^{Col1CreERT} KO mice were confirmed by genotyping and immunohistochemical analysis of the harvested tibiae. These mice were crossed to immunodeficient mice so that they could grow human tumors. The bones of the *Tgfbr2*^{Col1CreERT} KO mice were normal, as analyzed by X-ray (no bone lesions or fractures), microCT (for bone mineral density, cortical and trabecular bones, cross-sectional bone thickness and parameter), and histomorphometry (for the number of osteoclasts and osteoblasts) (5). In this study, the mice were crossed to the NSG-SCID mouse background, so C4-2B PCa cells could grow in the bones. The research using these mice was approved by the Van Andel Institute (VAI) Institutional Animal Care and Use Committee (IACUC) under protocol numbers 19-01-002 and 10-01-001.

Mouse osteoblast MC3T3-E1 cells and human osteoblast hFOB1.19 cells were from Dr.Bart Williams' lab of VAI, mouse macrophage RAW264.7 (used for osteoclasts) cells were from Dr. Cindy Miranti's lab at Arizona State University, and human PCa C4-2B cells were obtained from Dr. Leland Chang at Cedars Sinai. C4-2B/TGFBR2 cells were generated using an expression construct that was kindly provided by Dr. Jindan Yu at Northwest University. All cells were grown in a humidified incubator with 5% CO_2 at 37 °C, except for hFOB1.19 cells which were

grown at 34 °C. The cells were periodically checked for mycoplasma contamination, and only mycoplasma-free cells were used for experiments.

Enzalutamide was purchased from Selleckchem and Sigma-Aldrich. Abiraterone was purchased from Selleckchem. XC039 or XC, the PTH1R small-molecule inhibitor, was provided by Dr. Eric Xu (Van Andel Institute). These drugs were all dissolved in DMSO at various concentrations for *in vitro* studies. For *in vivo* studies, enzalutamide was dissolved in vehicle, 15% DMSO + 85% PEG300. The peptide antagonist for PTH1R (H-3274), (Asn^{10}, Leu^{11}, D-Trp^{12}) PTHrP (7–34) amide, and neutralizing antibody of PTHrP (T4512) were purchased from Bachem. TGF-β1 was purchased from R&D (240-B).

Experimental mouse models

NSG-SCID male mice, 6-8 weeks old, were purchased from the vivarium of VAI for use in this study. For subcutaneous xenograft models, 1 million C4-2B cells were suspended in 100 μL of Matrigel and subcutaneously injected into the flank of NSG-SCID mice. Tumors were measured twice per week using digital calipers. Tumor volume was calculated using the formula $V = (a^2 \times b)/2$, a and b indicating the minimal and maximal diameter, respectively. When the volume of subcutaneous tumors reached 100 mm^3, mice were randomized into a treatment group (enzalutamide at 20 mg/kg body weight once per day through oral gavage) or a vehicle group (given the same volume of the vehicle, 15% DMSO + 85% PEG300, once per day via oral gavage). For orthotopic xenograft models, 1 million C4-2B cells were suspended in 10 μL of PBS and injected into the anterior lobe of the mouse prostate. Tumors were monitored once per

week by bioluminescent imaging. Enzalutamide treatments started when the bioluminescent signals of orthotopic tumors were comparable to the signals from 100-mm^3 subcutaneous tumors. For intratibial injection, 1 million C4-2B cells in 10 μL of PBS were injected into the mouse tibiae as described previously (5). The injected mice were then randomized and started on drug treatment the next day. Bone lesions and tumor growth were monitored once per week by radiographic imaging using a Faxitron X-ray machine and bioluminescent imaging using an AMI-1000, respectively. The bone lesion areas and regions of interest (ROIs) were measured using MetaMorph (Molecular Devices Inc.).

All cell preparations, injections, imaging, tumor measurements, and bone lesion analyses were performed blinded.

Western blotting

Cells were lysed with RIPA lysis buffer containing Roche's Complete Proteinase Inhibitor Cocktail Tablets. The total protein was quantified using the BCA protein quantitative method according to the manufacturer's protocol. Approximately 10-40 μg protein per sample was loaded and electrophoresed through 10% or 12% SDS polyacrylamide gels and transferred onto nitrocellulose membranes. The membranes were then incubated overnight at 4 °C with primary antibodies for TGFBR2 (1:1000, Santa Cruz # sc-17792), p-Smad2 (1:1000, Cell Signaling # 3108), PTH1R (1:500, Abcam # 180762), NR2F1 (1:1000, Cell Signaling # 6364) or AR (1:500, Santa Cruz # sc-816). GAPDH (1:10,000, Cell Signaling # 5174), β-actin (1:5000, Sigma # A5441), or β-tubulin (1:5000, Sigma # T4026) was used as the loading control. HRP-conjugated secondary antibodies (goat-anti-mouse # 31430 and goat-anti-rabbit # 31460, diluted 1:5000-

10,000) and enhanced chemiluminescence (ECL) HRP substrate (# 34076) were purchased from ThermoFisher Scientific.

CRISPR/Cas9-based gene editing of *Ar* in MC3T3-E1 cells

Single guide RNAs (sgRNA) for mouse *Ar* were designed and ordered from Synthego. Ribonucleoprotein (RNP) complexes that consist of purified Cas9 nuclease duplexed with synthetic sgRNA were prepared and delivered to MC3T3-E1 cells using Lipofectamine CRISPRMAX Transfection Reagent (Invitrogen). Cells were harvested and western blots were used to confirm the gene knockdown and TGFBR2 regulation after 3 days.

Tissue microarray, histology, and immunohistochemistry

The PCa metastasis tissue microarray (TMA) UWTMA79 was obtained from the University of Washington. This TMA contained samples from 45 cases of bone and visceral metastasis from rapid autopsy (62 visceral and 79 bone metastasis). The slides were subjected to immunohistochemical analysis of TGFBR2, as described previously. The stained slides were digitally captured and quantified independently by the pathologist using a score of 0 to 3 in various cell types for intensities of negative, moderate, and strong. The scores were submitted to the Bioinformatics and Biostatistics Core for discovery analyses of correlations among the cell-specific expression of TGFBR2 and any of the clinical parameters.

Subcutaneous or orthotopic C4-2B tumors, as well as C4-2B injected tibiae, were harvested at the endpoints and fixed in 10% neutral-buffered formalin for 2 d. After fixation, the tibiae were processed to decalcification in 14% EDTA for 5-6 days. All the steps were performed at 4 °C. The tissues were then paraffin-embedded. Paraffin-embedded sections (5 μm) were

deparaffinized and stained with hematoxylin and eosin (H&E). For immunohistochemistry, paraffin-embedded sections were subjected to standard peroxidase-based immunohistochemistry procedures. The TGFBR2 antibody (Santa Cruz # sc-17792) was used with 1:50 dilution.

RNA extraction and qRT-PCR

Total RNA was isolated using TRIzol (Invitrogen) and subsequently purified using the RNeasy kit (Qiagen). Complementary DNA was synthesized using a SuperScript VILO cDNA Synthesis Kit (Invitrogen), and qRT-PCR was performed using SYBR Select Master Mix (Bio-Rad) with an ABI 7500 machine (Applied Biosystems). Cycle threshold values were determined and normalized to the loading control, *Gapdh*, for each experiment. Fold changes for experimental groups were calculated using the $\Delta\Delta C_T$ method. The primer sequences are listed in **Supplementary Table 2**.

Chromatin immunoprecipitation (ChIP) analysis

ChIP analysis was conducted with a Simple ChIP Kit from Cell Signaling Technology (#9003), following the manual. Briefly, 4 million adherent MC3T3 cells treated with either vehicle (DMSO) or enzalutamide were rinsed with ice-cold PBS once to remove the residual culture medium and then were fixed with 1% formaldehyde in PBS at room temperature for 15 min on a gentle horizontal shaker. Glycine was then introduced into the solution for 5 min to terminate the fixation. The liquid was aspirated, and the cells were rinsed twice with cold PBS. The cells were scraped with cold PBS and centrifuge at 500 × *g* and 4 °C for 2 min to pellet the cells. Then the cells were lysed, digested with MNase, and sonicated to release the chromatin. After confirmation of the fragmentation, the chromatin was diluted and incubated with NR2F1

antibody (10 μL) or isotype control IgG overnight. The antibody-enriched chromatin was then pelleted by magnet beads and purified with spin columns included in the kit. Fold enrichment of NR2F1 on the *Pth1r* promoter was determined by qPCR. The primer sequences are listed in **Supplementary Table 2**.

Statistical analysis

Clinical data were first input using a random forest iterated for 5 times, with 300 trees each. Then, LASSO (least absolute shrinkage and selection operator) analyses were used to explore any associations between clinical data and cell-specific TGFBR2 expression in PCa patient bone metastasis tissues. Experimental data are presented as mean ± SEM. Longitudinal bone lesion data were analyzed via a linear mixed-effect model. Linear contrasts with a false discovery rate correction were used to test for significant differences in bone lesion growth rates, and bootstrap hypothesis testing with 1000 resampled data sets was used to test for differences in total lesion area between groups at specific time points. For experiments without repeated measures, data were analyzed via two-way ANOVA when there were two independent variables; otherwise, a two-tailed Student's *t*-test was used. Normality assumptions were assessed visually via QQ-plots; no concerning deviations were detected. For bone lesion proportion analysis, we performed a two-tailed t-test on the incidence of bone lesions in the two groups. *t*-tests and ANOVAs were performed in Graphpad and all other analyses in R v 3.2.2. For all analyses, $p < 0.05$, two-sided, was considered significant.

Author contributions

XL conceived and directed the project. XL, SS, and JC wrote the manuscript. XL, SS, JC, and XM designed the experiments and analyzed the data with help from RL, AVA, EW, RZ, and IS. XZ scored the cell-specific TGFBR2 expression in tissue microarray. ZM performed the statistical analyses. MB conducted the MetaCore analysis. EX and HY provided resources.

Acknowledgements

We thank Drs. Bart Williams, Patrick Grohar, Tao Yang, Matt Steensma, and their lab members for intriguing discussion and technical help, Dr. Yingying Wu for helpful suggestions on statistical analysis and language revision, and David Nadziejka for technical editing. This work was supported by NCI grant R01CA230744 and a grant from Van Andel Institute (50310A) to XL. The prostate cancer bone metastasis tissue microarray was purchased from the Prostate Cancer Biorepository Network, which is funded by W81XWH-14-2-0182, W81XWH-14-2-0183, W81XWH-14-2-0185, W81XWH-14-2-0186, and W81XWH-15-2-0062.

Figure Legends

Figure 1. Enzalutamide treatment was effective in subcutaneous models of prostate cancer but not in intratibial models. A) Enzalutamide treatment significantly inhibited C4-2B subcutaneous tumor growth. Subcutaneous tumor volume progression and representative pictures of individual tumors are shown. The bold lines are the mean values of the individual curves of each color. These parallel experiments were repeated twice with the same results. Enzalutamide dissolved in vehicle (15% DMSO + 85% PEG300), or vehicle alone was administered by oral gavage. Two weeks of treatments were started on day 21 when the tumor volume reached 100 mm^3. Tumor size was measured twice per week. A linear mixed-effect model, * $p = 0.001$, $n \geq 5$. **B)** Enzalutamide treatment had no effect on C4-2B–induced bone lesion development. Bone lesions were imaged by X-ray weekly, and lesion areas were measured using Metamorph software. The lesion areas measured are outlined. Treatments were started on day 2 after cancer cell injections. A linear mixed-effect model, $p = 0.793$, $n \geq 8$; n.s., non-significant.

Figure 2. Enzalutamide decreased TGFBR2 in osteoblasts. A) Time- and dose-dependent **effects.** 0 = vehicle (DMSO). **B)** AR-dependent effect of TGFBR2. The mixed cell populations (but not selected single-cell clones) of *Ar* knockdown (KD) were achieved using the CRISPR-Case9 system. The control was cells transfected without guide RNA. Total protein was extracted from cells for western blotting. Experiments were repeated three times with the same results. **C)** The human osteoblast cell line hFOB1.19 was treated as indicated. Experiments were repeated twice with the same results. **D & E)** Enzalutamide or abiraterone treatment in patients was associated with lower TGFBR2 expression in osteoblasts. **D)** Representative IHC images of

TGFBR2 in osteoblasts. Lines in zoomed lower panel highlight osteoblasts. PCa, prostate cancer cells; B, bone Scale bar, upper panel 300 μm, lower panel 50 μm. **E)** IHC scores were significantly lower in patients who received enzalutamide or abiraterone treatment than in patients receiving neither treatment after ADT. * $p = 0.03$ using a linear mixed-effect model.

Figure 3. Enzalutamide-induced TGFBR2 down-regulation was mediated by PTH1R. A) TGFBR2 down-regulation with PTH1R. MC3T3-E1 cells were treated with 10 μg/mL cycloheximide (CHX), 1 ng/mL TGF-β, or 100 nM PTHrP at the indicated times. Total protein extractions from cells were used for western blotting. **B & C)** Enzalutamide increased PTH1R at the protein **(B)** and mRNA **(C)** levels prior to the decrease of TGFBR2. MC3T3-E1 cells were treated with vehicle (-, DMSO) or enzalutamide (enz, 40 μM). Total proteins were extracted from cells for western blotting. The scatter plot in **C** displayed mean and individual values generated from multiple independent repeat experiments. * indicates $p < 0.05$, by t-test. **D)** Blockade of PTH1R rescued the TGFBR2 loss upon enzalutamide treatment. MC3T3 cells were treated with vehicle, DMSO; Ant, the peptide antagonist for PTH1R; Ab, the neutralizing antibody of PTHrP; or XC, the small-molecule inhibitor of PTH1R for 24 h before immunoblotting. All the experiments were repeated three times with the same results.

Figure 4. Enzalutamide induced NR2F1 expression and recruitment on the Pth1r promoter. A) NR2F1 was identified as a potential transcription factor responsible for PTH1R transcriptional activation upon AR signaling blockade**. B &C)** Enzalutamide up-regulated NR2F1 at both the mRNA **(B)** and protein levels **(C)** in osteoblasts**.** MC3T3 cells were treated with vehicle (-, DMSO) or enzalutamide (enz, 40 μM) for the indicated hours before harvest for

immunoblotting or RNA extraction. The scatter plot in **B** displayed mean and individual values generated from multiple independent repeat experiments. * indicates $p < 0.05$, by t-test. **D)** Enzalutamide increased the occupancy of NR2F1 at the *Pth1r* promoter**.** NR2F1 binding elements appear frequently across *Pth1r* promoter(s) of different *Pth1r* transcript variants (V1, V2, and V3). ChIP assay with different targeting primers (amplicons termed as c1, c2, and c3) all showed an increase in NR2F1 occupancy on *Pth1r* regulatory regions upon enzalutamide treatment. **E)** Proposed mechanism of enzalutamide resistance in bone metastasis. In a responsive microenvironment, such as the prostate and subcutaneous region, enzalutamide blocks AR and suppress PCa tumor growth. In bone, enzalutamide blocks AR and removes the suppression of AR on NR2F1 expression. Elevated NR2F1 is then recruited onto the *Pth1r* promoter, which stimulates the expression of PTH1R. The PTH1R proteins induce the degradation of TGFBR2 in osteoblasts to promote prostate cancer bone metastasis.

Supplementary Figure 1

Orthotopic tumors grown in the mouse prostate were imaged using bioluminescence once per week and analyzed using a linear mixed-effect model. $p \leq 0.023$, $n \geq 4$. The treatments were started on day 15 when the bioluminescent signals of orthotopic tumors were comparable to the signals from 100-mm^3 subcutaneous tumors.

Supplementary Figure 2

A) Representative X-rays of mixed bone lesions of C4-2B cells after 4, 6, and 8 weeks post intratibial injection. **B)** The proportion of mice with detectable C4-2B cell-induced bone lesions was significantly higher ($p<0.001$) in the *Tgfbr2*^{Col1CreERT} KO group relative to the *Tgfbr2*^{Flox} control group. The number of mice with detectable bone lesions identified by X-ray scanning of each group was counted 8 weeks after injection. The growth of C4-2B cells was confirmed by H&E staining.

Supplementary Figure 3

Raw264.7 cells **(A)** and C4-2B/TGFBR2 cells **(B)** were treated with enzalutamide (enz) or vehicle (DMSO) for 4 h, 6 h, or 24 h before harvest for western blotting. Samples were blotted with TGFBR2, PTH1R, NR2F1, and GAPDH (loading control).

Supplementary Table 1

Cell-specific TGFBR2 staining scores for the tissues from the bone metastatic tissue microarray.

Supplementary Table 2

Primer sequences used in this study.

References

1. Feng Q, and He B. Androgen Receptor Signaling in the Development of Castration-Resistant Prostate Cancer. *Front Oncol.* 2019;9:858.
2. Karantanos T, Corn PG, and Thompson TC. Prostate cancer progression after androgen deprivation therapy: mechanisms of castrate resistance and novel therapeutic approaches. *Oncogene.* 2013;32(49):5501-11.
3. Vander Ark A, Cao J, and Li X. Mechanisms and Approaches for Overcoming Enzalutamide Resistance in Prostate Cancer. *Front Oncol.* 2018;8:180.
4. Goh P, Harris K, Napolskikh J, Chow E, Sinclair E, Emmenegger U, et al. New multidisciplinary prostate bone metastases clinic: first of its kind in Canada. *Curr Oncol.* 2007;14(1):9-12.
5. Meng X, Vander Ark A, Daft P, Woodford E, Wang J, Madaj Z, et al. Loss of TGF-beta signaling in osteoblasts increases basic-FGF and promotes prostate cancer bone metastasis. *Cancer Lett.* 2018;418:109-18.
6. Ylitalo EB, Thysell E, Jernberg E, Lundholm M, Crnalic S, Egevad L, et al. Subgroups of Castration-resistant Prostate Cancer Bone Metastases Defined Through an Inverse Relationship Between Androgen Receptor Activity and Immune Response. *Eur Urol.* 2017;71(5):776-87.
7. Cunningham D, and You Z. In vitro and in vivo model systems used in prostate cancer research. *J Biol Methods.* 2015;2(1).
8. Ganguly SS, Li X, and Miranti CK. The host microenvironment influences prostate cancer invasion, systemic spread, bone colonization, and osteoblastic metastasis. *Frontiers in oncology.* 2014;4:364.
9. Park SH, Keller ET, and Shiozawa Y. Bone Marrow Microenvironment as a Regulator and Therapeutic Target for Prostate Cancer Bone Metastasis. *Calcif Tissue Int.* 2018;102(2):152-62.
10. Sedelaar JP, and Isaacs JT. Tissue culture media supplemented with 10% fetal calf serum contains a castrate level of testosterone. *Prostate.* 2009;69(16):1724-9.
11. Larson SR, Zhang X, Dumpit R, Coleman I, Lakely B, Roudier M, et al. Characterization of osteoblastic and osteolytic proteins in prostate cancer bone metastases. *Prostate.* 2013;73(9):932-40.
12. Rehman Y, and Rosenberg JE. Abiraterone acetate: oral androgen biosynthesis inhibitor for treatment of castration-resistant prostate cancer. *Drug Des Devel Ther.* 2012;6:13-8.
13. Qiu T, Wu X, Zhang F, Clemens TL, Wan M, and Cao X. TGF-beta type II receptor phosphorylates PTH receptor to integrate bone remodelling signalling. *Nature cell biology.* 2010;12(3):224-34.
14. Wysolmerski JJ. Parathyroid hormone-related protein: an update. *J Clin Endocrinol Metab.* 2012;97(9):2947-56.
15. Pioszak AA, Parker NR, Gardella TJ, and Xu HE. Structural basis for parathyroid hormone-related protein binding to the parathyroid hormone receptor and design of conformation-selective peptides. *The Journal of biological chemistry.* 2009;284(41):28382-91.
16. Xu P, Liu J, and Derynck R. Post-translational regulation of TGF-beta receptor and Smad signaling. *FEBS Lett.* 2012;586(14):1871-84.

17. Karperien M, Farih-Sips H, Hendriks JA, Lanske B, Papapoulos SE, Abou-Samra AB, et al. Identification of a retinoic acid-inducible element in the murine PTH/PTHrP (parathyroid hormone/parathyroid hormone-related peptide) receptor gene. *Mol Endocrinol.* 1999;13(7):1183-96.
18. Perets R, Kaplan T, Stein I, Hidas G, Tayeb S, Avraham E, et al. Genome-wide analysis of androgen receptor targets reveals COUP-TF1 as a novel player in human prostate cancer. *PLoS One.* 2012;7(10):e46467.
19. Khan A, Fornes O, Stigliani A, Gheorghe M, Castro-Mondragon JA, van der Lee R, et al. JASPAR 2018: update of the open-access database of transcription factor binding profiles and its web framework. *Nucleic Acids Res.* 2018;46(D1):D260-D6.
20. Kawane T, Mimura J, Fujii-Kuriyama Y, and Horiuchi N. Identification of the promoter region of the parathyroid hormone receptor gene responsible for transcriptional suppression by insulin-like growth factor-I. *Arch Biochem Biophys.* 2005;439(1):61-9.

Figure 1

A

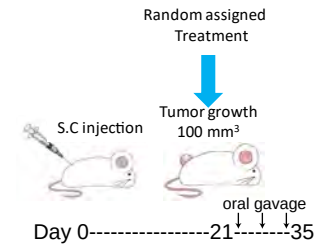
Random assigned
Treatment
S.C injection
Tumor growth
100 mm³
oral gavage
Day 0----------21-------35

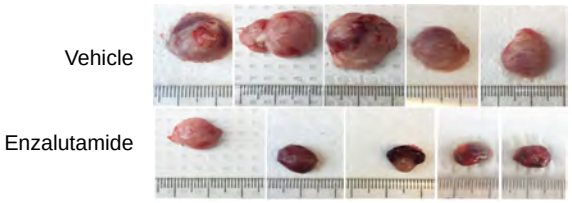
Vehicle
Enzalutamide

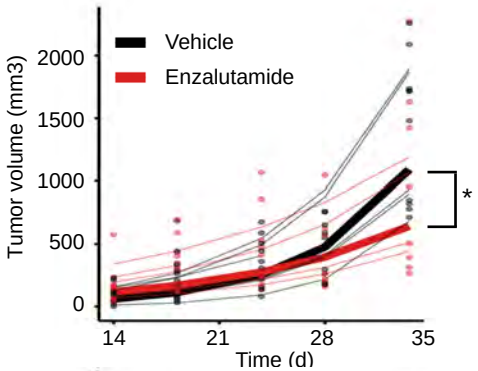
Vehicle
Enzalutamide
Tumor volume (mm3)
2000
1500
1000
500
0
14
21
28
35
Time (d)
*

B

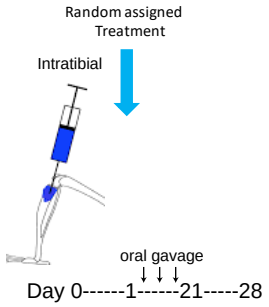
Random assigned
Treatment
Intratibial
oral gavage
Day 0------1------21-----28

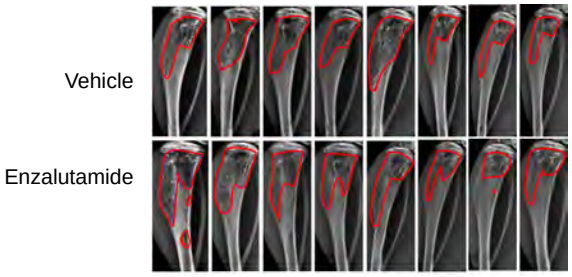
Vehicle
Enzalutamide

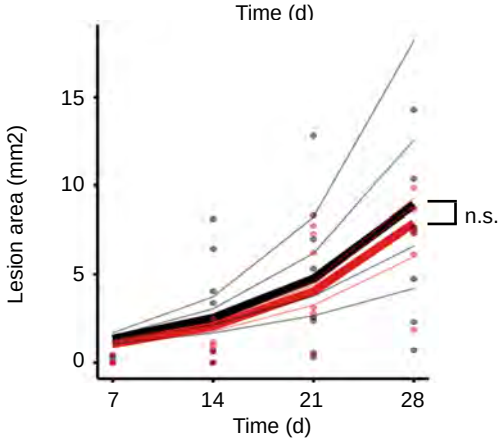
Lesion area (mm2)
15
10
5
0
7
14
21
28
Time (d)
n.s.

Figure 2

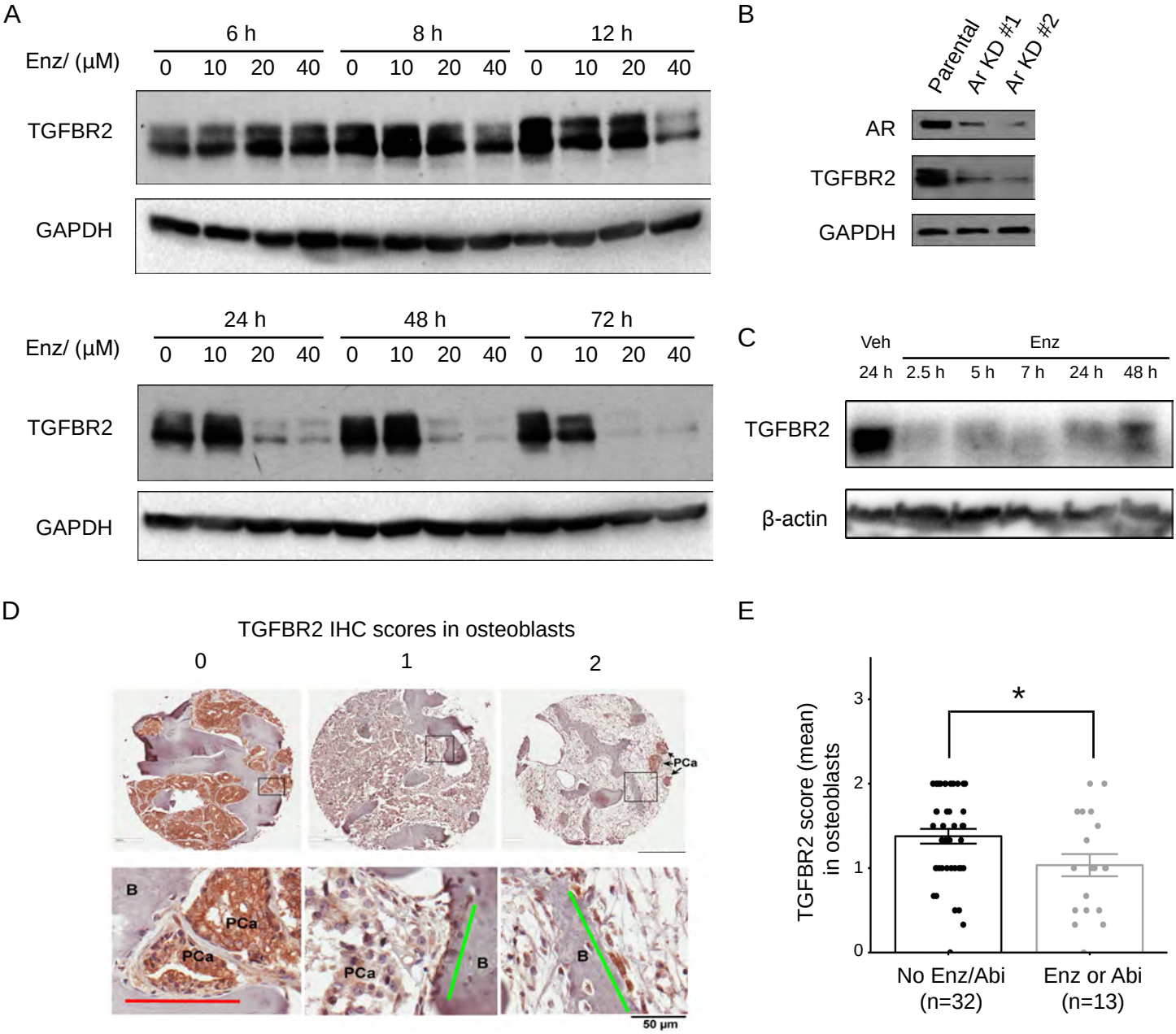
A
6 h
8 h
12 h
Enz/ (μM)
0 10 20 40 0 10 20 40 0 10 20 40
TGFBR2
GAPDH
24 h
48 h
72 h
Enz/ (μM)
0 10 20 40 0 10 20 40 0 10 20 40
TGFBR2
GAPDH
B
Parental
Ar KD #1
Ar KD #2
AR
TGFBR2
GAPDH
C
Veh
Enz
24 h 2.5 h 5 h 7 h 24 h 48 h
TGFBR2
β-actin
D
TGFBR2 IHC scores in osteoblasts
0
1
2
PCa
B
PCa
PCa
PCa
B
B
50 μm
E
TGFBR2 score (mean) in osteoblasts
0
1
2
3
*
No Enz/Abi (n=32)
Enz or Abi (n=13)

Figure 3

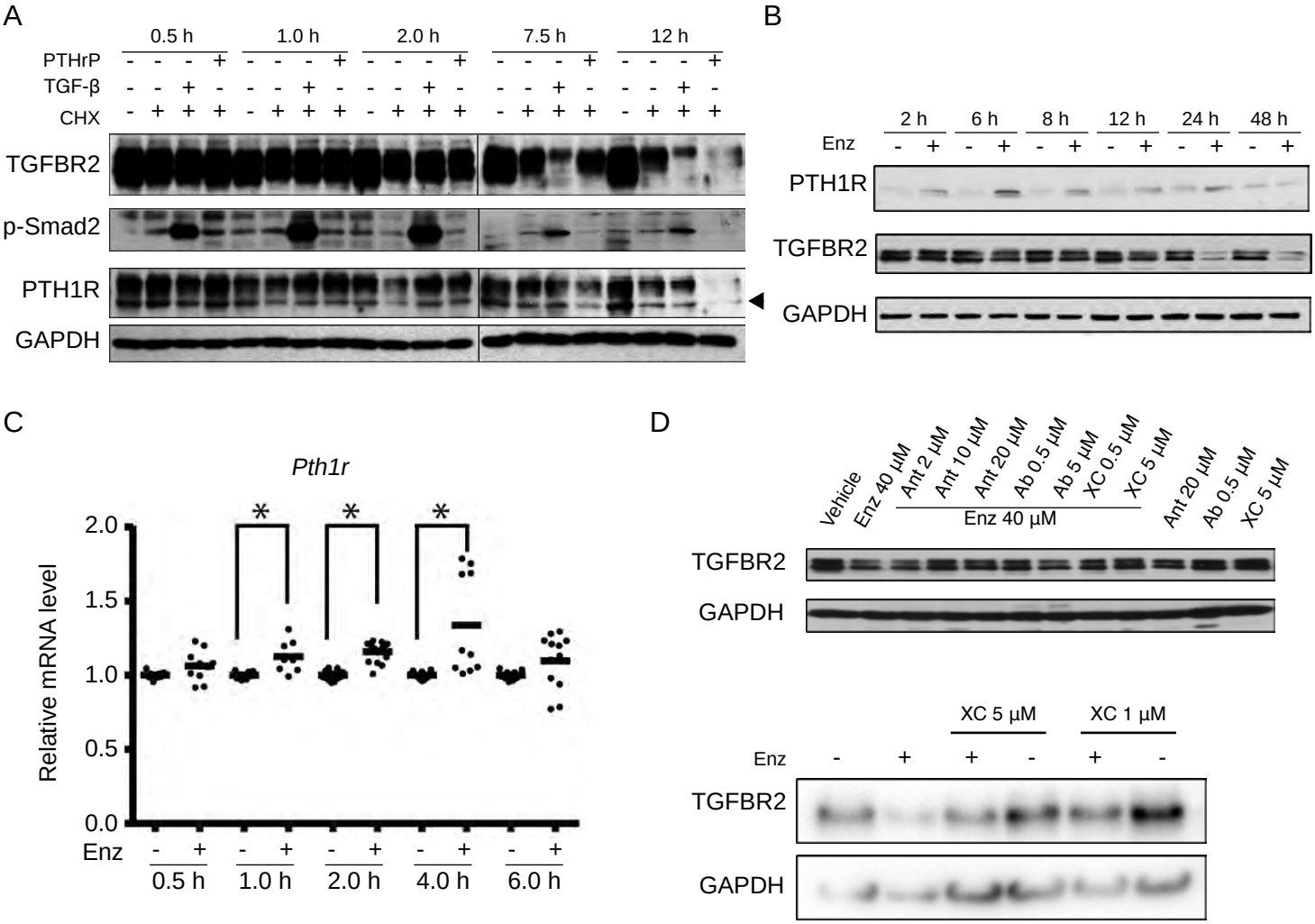
A
0.5 h
1.0 h
2.0 h
7.5 h
12 h
PTHrP
TGF-β
CHX
TGFBR2
p-Smad2
PTH1R
GAPDH
B
2 h
6 h
8 h
12 h
24 h
48 h
Enz
PTH1R
TGFBR2
GAPDH
C
Pth1r
Relative mRNA level
2.0
1.5
1.0
0.5
0.0
Enz
0.5 h
1.0 h
2.0 h
4.0 h
6.0 h
D
Vehicle
Enz 40 μM
Ant 2 μM
Ant 10 μM
Ant 20 μM
Ab 0.5 μM
Ab 5 μM
XC 0.5 μM
XC 5 μM
Enz 40 μM
Ant 20 μM
Ab 0.5 μM
XC 5 μM
TGFBR2
GAPDH
XC 5 μM
XC 1 μM
Enz
TGFBR2
GAPDH

Figure 4

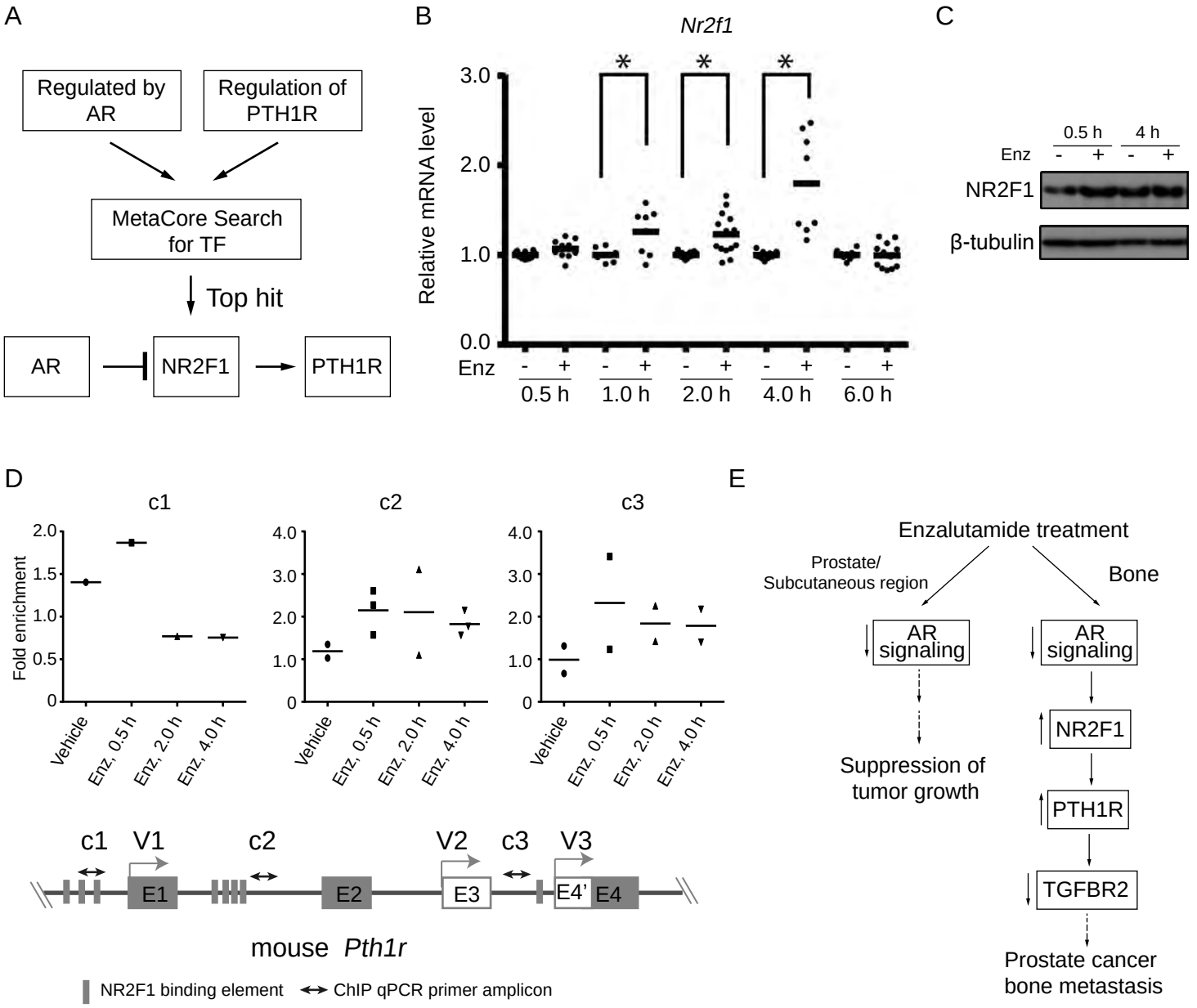
A
Regulated by AR
Regulation of PTH1R
MetaCore Search for TF
Top hit
AR
NR2F1
PTH1R
B
Nr2f1
Relative mRNA level
3.0
2.0
1.0
0.0
Enz
0.5 h
1.0 h
2.0 h
4.0 h
6.0 h
C
0.5 h
4 h
Enz
NR2F1
β-tubulin
D
c1
c2
c3
Fold enrichment
Vehicle
Enz, 0.5 h
Enz, 2.0 h
Enz, 4.0 h
V1
V2
V3
E1
E2
E3
E4'
E4
mouse Pth1r
NR2F1 binding element
ChIP qPCR primer amplicon
E
Enzalutamide treatment
Prostate/ Subcutaneous region
Bone
AR signaling
NR2F1
PTH1R
TGFBR2
Suppression of tumor growth
Prostate cancer bone metastasis